Chinese Chemical Letters 36 (2025) 109874

Contents lists available at ScienceDirect

Chinese Chemical Letters

journal homepage: www.elsevier.com/locate/cclet

GSH-activatable copper-elsinochrome off-on photosensitizer for combined specific NIR-II two-photon photodynamic/chemodynamic therapy

Zekun Gao[a,b], Xiuli Zheng[a,*], Weimin Liu[a,b], Jie Sha[a,b], Shuaishuai Bian[a,b], Haohui Ren[a], Jiasheng Wu[a], Wenjun Zhang[c], Chun-Sing Lee[c], Pengfei Wang[a,b,*]

[a] Key Laboratory of Photochemical Conversion and Optoelectronic Materials and CityU-CAS Joint Laboratory of Functional Materials and Devices, Technical Institute of Physics and Chemistry, Chinese Academy of Sciences, Beijing 100190, China
[b] School of Future Technology, University of Chinese Academy of Sciences, Beijing 100049, China
[c] Center of Super-Diamond and Advanced Films (COSDAF) & Department of Materials Science and Engineering, City University of Hong Kong, Hong Kong SAR 999077, China

ARTICLE INFO

Article history:
Received 24 January 2024
Revised 2 April 2024
Accepted 8 April 2024
Available online 9 April 2024

Keywords:
GSH activation
Copper-elsinochrome photosensitizer
Reactive oxygen species
NIR-II two-photon photodynamic therapy
Chemodynamic therapy

ABSTRACT

The complexity of cancer therapy has led to the emergence of combination therapy as a promising approach to enhance treatment efficacy and safety. The integration of glutathione (GSH)-activatable two-photon photodynamic therapy (TP-PDT) and chemodynamic therapy (CDT) offers the possibility to advance precision and efficacy in anti-cancer treatments. In this study, a GSH-activatable photosensitizer (PS), namely copper-elsinochrome (CuEC), is synthesized and utilized for combination second near-infrared (NIR-II) TP-PDT/CDT. The Cu^{2+} acts as a "lock", suppressing the fluorescence and $^1O_2$ generation ability of EC in a normal physiological environment ("OFF" state). However, the overexpressed GSH in the tumor microenvironment acts as the "key", resulting in the release of EC ("ON" state) and Cu^{+} (reduced by GSH). The released EC can be utilized for fluorescence imaging and TP-PDT under NIR-II ($\lambda = 1000$ nm) two-photon excitation, while Cu^{+} can generate highly toxic hydroxyl radicals ($^{\bullet}OH$) *via* Fenton-like reaction for CDT. Additionally, this process consumes GSH and diminishes the tumor's antioxidant capacity, thereby augmenting the efficacy of combination therapy. The CuEC achieves significant tumor cell ablation in both 2D monolayer cells and 3D multicellular tumor spheres through the combination of NIR-II TP-PDT and CDT.

Induction of cell death through reactive oxygen species (ROS) is a widely employed strategy in cancer therapy, including modalities such as radiotherapy (RT), photodynamic therapy (PDT), sonodynamic therapy (SDT), and chemodynamic therapy (CDT) [1,2]. Among them, PDT is considered as a promising treatment strategy in the field of anti-tumor due to its advantages of excellent selectivity, minimal side effects, and low invasiveness [3,4]. PDT is a process in which photosensitizer (PS) convert surrounding O_2 or substrate into ROS under light irradiation to kill cancer cells [5–7]. Due to the limited absorption wavelength range of traditional PSs, their application is primarily restricted to the treatment of superficial and cavity-type tumors, such as skin cancer and esophageal cancer [8,9]. To overcome this challenge, researchers have developed PSs based on up-conversion [10,11], near-infrared (NIR) [12,13], and two-photon excitation (TPE) [14,15] to achieve enhanced tissue penetration. Among these, TPE PSs have gained increasing attention in the field of biomedicine due to their ability to retain one-photon (OP) absorption and exhibit exceptional spatial accuracy [16,17]. Unlike one-photon excitation (OPE), TPE technology utilizes a pair of longer-wavelength photons simultaneously to excite the PS during the treatment process [18,19]. This results in a significant increase in tissue penetration depth and imaging resolution, while reducing laser-induced damage to neighboring healthy tissues [20,21]. However, two-photon photodynamic therapy (TP-PDT) also encounters the challenge of hypoxia within the tumor microenvironment (TME) [12,22]. Therefore, the integration of TP-PDT with other therapeutic modalities holds great potential for enhancing the overall efficacy of tumor treatment.

The CDT enables the conversion of endogenous hydrogen peroxide (H_2O_2) at the tumor site into cytotoxic hydroxyl radicals

* Corresponding authors.
E-mail addresses: zhengxiuli@mail.ipc.ac.cn (X. Zheng), wangpf@mail.ipc.ac.cn (P. Wang).

https://doi.org/10.1016/j.cclet.2024.109874
1001-8417/

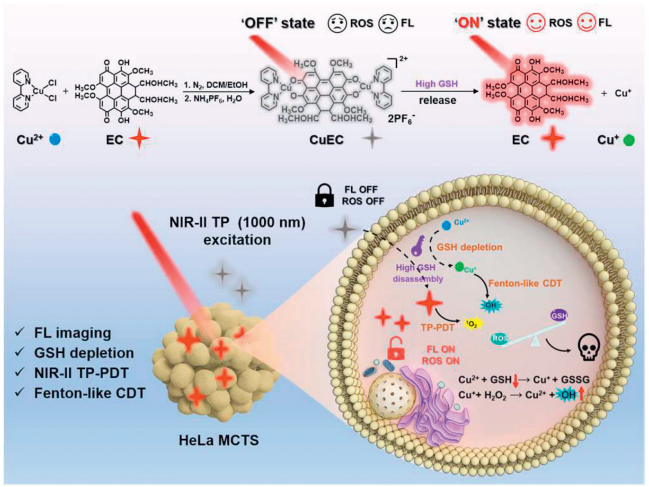

Scheme 1. Illustration of CuEC as a GSH-activatable PS for combined specific NIR-II TP-PDT/CDT.

(•OH), thereby partially mitigating the limitation of PDT, which relies on O_2 [23,24]. Moreover, the emergence of activatable theranostic agents has accelerated the application of fluorescence imaging in tumor diagnosis and therapeutic monitoring, thereby augmenting the specificity of tumor diagnosis and the effectiveness of therapeutic outcomes [25]. These activatable theranostic agents can be precisely activated within the TME, such as hypoxia, overexpressed H_2O_2 and glutathione (GSH), offering a strategic advantage for targeted therapy. This approach not only maximizes therapeutic efficacy but also minimizes damage to healthy tissues [26,27]. Cu, which serves as a cofactor for redox-active Cu-dependent enzymes, is essential in numerous biological processes [28]. The increasing evidence suggests that GSH possesses the capability to facilitate the reduction of Cu^{2+}, leading to the formation of Cu^{+} species [29]. These Cu^{+} act as Fenton-like reagent for the conversion of H_2O_2 into •OH [30,31]. Additionally, the decrease in GSH levels induced by Cu^{2+} has been shown to intensify oxidative stress within cancer cells, thereby enhancing its anticancer effect [32,33]. Under typical physiological conditions, Cu^{2+} coordination with suitable PSs results in the formation of highly stable Cu^{2+}/PS prodrug. Due to energy transfer or electron transfer interactions between Cu^{2+} and PSs, these prodrugs remain in an "OFF" state [34–36], characterized by the fluorescence quenching of PSs and the inability to generate ROS under laser irradiation. However, in the TME, Cu^{2+}/PS prodrug tend to undergo disaggregation due to the high concentration of GSH (1–10 mmol/L) [37,38]. This disaggregation occurs due to the reaction between Cu^{2+} and GSH, resulting in the selective release of Cu^{+} and PS within the tumor cells. The released PS could generate ROS under laser irradiation for PDT, and the released Cu^{+} could initiate Fenton-like reactions to induce CDT effects. The combination of PDT and CDT, therefore, holds great potential in enhancing the efficacy of malignant tumor treatment and represents a promising approach to achieving optimal therapeutic outcomes.

Elsinochrome is a type of natural perylenequinonoid PS with advantages such as high singlet oxygen ($^1O_2$) quantum yield (as high as 0.98, with hypocrellin B (0.84) in benzene as a reference [39]), low toxicity, and fast metabolism *in vivo* [40,41]. The presence of a large conjugated π-electron system in elsinochrome enables it to exhibit significant TP absorbance, making it well-suited for TP-PDT [42,43]. Additionally, the structure of elsinochrome C (EC) contains phenolic hydroxyl and quinonoid carbonyl oxygens, which serve as binding sites for Cu^{2+} chelation [44]. Herein, we developed a novel GSH-activatable prodrug, named CuEC, for the combination NIR-II TP-PDT/CDT therapy (Scheme 1). The CuEC can

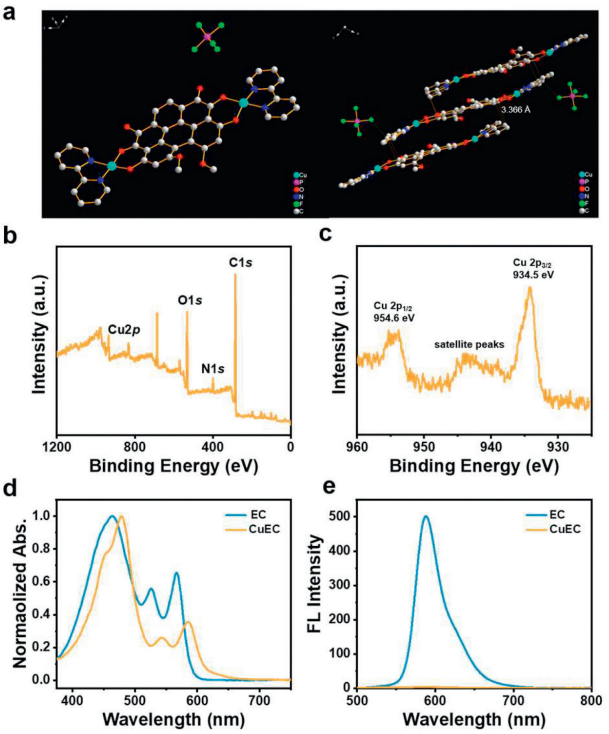

Fig. 1. (a) Crystal structure and molecular packing of CuEC (hydrogen atom is omitted for clarity). (b) XPS survey spectra of CuEC. (c) Cu 2p XPS spectra of CuEC. (d) Normalized ultraviolet–visible (UV–vis) absorbance spectra of EC and CuEC in DMSO. (e) Fluorescence spectra of EC and CuEC (10 μmol/L, DMSO, λ_{ex} = 480 nm).

be activated to an "ON" state by overexpressed GSH in the TME, resulting in the release of EC and Cu^{+}. The released EC can fluoresce for FL imaging and generate $^1O_2$ for TP-PDT under NIR-II TP laser irradiation. Additionally, the released Cu^{+} can react with overexpressed H_2O_2 through a Fenton-like reaction, generating toxic •OH. This process depletes GSH and reduces the tumor's antioxidant activity, thereby enhancing the effectiveness of combination therapy. *In vitro* experiments have demonstrated that CuEC achieves significant tumor cell ablation in both 2D monolayer cells and 3D multicellular tumor sphere (MCTS) through the combination of NIR-II TP-PDT and CDT. This offers a promising approach for designing activatable PSs and treating deep-seated tumors.

The CuEC was synthesized by reacting EC with (2,2′-bipyridine)-dichlorocopper at room temperature under N_2 atmosphere. The synthetic and chemical structure of CuEC is shown in Scheme 1, while detailed experimental information is provided in Supporting information. The structure of CuEC was confirmed by means of single-crystal X-ray crystallography and ESI-MS (Fig. 1a and Fig. S1 in Supporting information). As shown in Fig. 1a, CuEC is a binuclear Cu(II) complex with EC as the bridging ligand and 2,2′-bipyridine as the terminal ligand, exhibiting an overall planar structure. CuEC molecules have a layer-by-layer packing mode through π-π stacking interaction (3.366 Å). Furthermore, the Cu content was accurately quantified using inductively coupled plasma mass spectrometry (ICP-MS), resulting in a measured value of 9.78%, which closely corresponds to the calculated value of 9.74%. The valence state of Cu in the CuEC compound was determined using X-ray photoelectron spectroscopy (XPS). The presence of Cu, C, N, and O elements in the CuEC was observed in Fig. 1b. The peaks corresponding to Cu ($2p_{3/2}$) and Cu ($2p_{1/2}$) in Cu^{2+} were identified at 934.5 and 954.6 eV, respectively. Furthermore, the presence of satellite peaks around 943.2 eV confirmed the existence of Cu^{2+} in the compound (Fig. 1c) [45–47]. The absorption band at 460 nm attributed to EC is assigned to the π-π^*

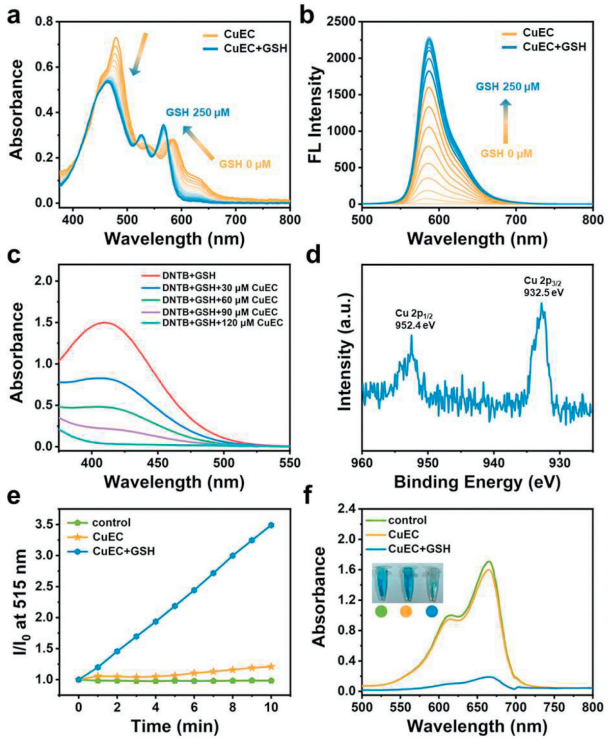

Fig. 2. (a) The absorbance spectra and (b) fluorescence spectra of CuEC (20 μmol/L, DMSO, λ_{ex} = 480 nm) upon treatment with different concentrations GSH at room temperature. (c) GSH consumption ability with DTNB as an indicator. (d) Cu 2p XPS spectra of CuEC + GSH. ·OH detection using (e) HPF (5 μmol/L, phosphate-buffered saline) and (f) MB as indicators.

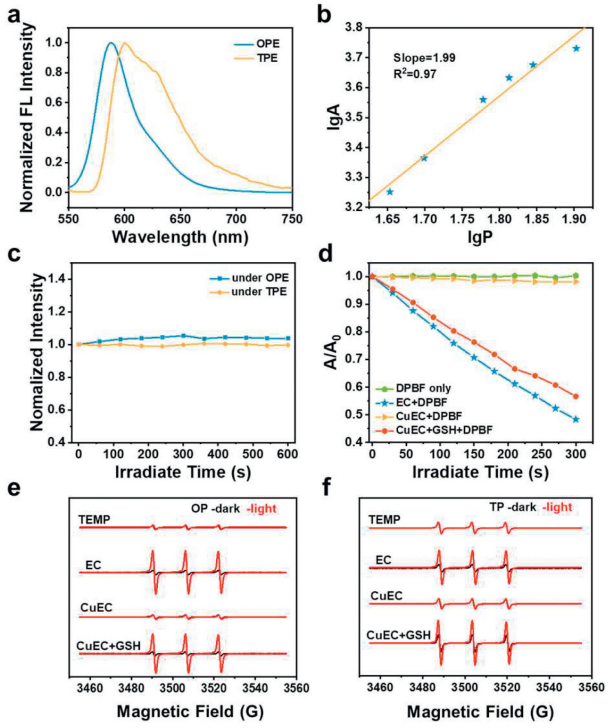

Fig. 3. (a) OPE (10 μmol/L) and TPE (1 mmol/L) fluorescence spectra of EC in DMSO at room temperature. (b) Quadratic correlation between the intensity of TP fluorescence and laser power. (c) Photostability of EC under two different laser conditions: 488 nm laser and 1000 nm fs laser. (d) $^1O_2$ detection using DPBF as an indicator under 532 nm laser irradiation. ESR spectra of $^1O_2$ with TEMP as a spin trapping reagent under (e) 532 nm laser irradiation and (f) NIR-II 1000 nm fs laser irradiation (100 mW/cm^2).

transition of the conjugated system consisting of the quinone carbonyl group and the perylene nucleus [48]. The coordination of Cu may promote the charge transfer (CT) process [44], therefore shifts the absorption maximum from 460 nm to longer wavelength (480 nm) (Fig. 1d). Compared to EC, the fluorescence of CuEC is completely quenched due to the paramagnetic nature of Cu [49] or as a result of Forster resonance energy transfer between EC and Cu^{2+} (Fig. 1e) [36].

Considering the internal overexpression of GSH in tumors, we next investigated the response behavior of CuEC under different concentrations of GSH. The changes in the absorbance spectra of CuEC in response to various concentrations of GSH are presented in Fig. 2a. Upon the addition of GSH, a gradual reduction in absorbance at 480 nm was observed, accompanied by an increase in absorbance at 565 nm. This resulted in an overall blue-shift in the absorbance spectra, ultimately aligning with the absorption spectrum of EC. Furthermore, the fluorescence of CuEC was gradually restored to the same fluorescence of EC with the addition of GSH (Fig. 2b). The ESI-MS results further demonstrated that the addition of GSH resulted in the formation of EC (Fig. S2 in Supporting information), indicating the effective activation of CuEC by GSH for EC release. As an indicator to quantify the consumption ability of GSH, 5,5′-dithiobis-2-nitrobenzoic acid (DTNB) can bind with free sulfhydryl groups (-SH) to form a yellow product, resulting in a characteristic absorbance peak at 412 nm [33,50]. As shown in Fig. 2c, the addition of CuEC resulted in a significant reduction in absorbance at 412 nm, indicating the ability of CuEC to effectively consume GSH. Next, we investigated the valence change of Cu in CuEC after the introduction of GSH. The disappearance of satellite peaks and the emergence of peaks at 932.5 and 952.4 eV confirmed the presence of Cu^+, thereby further substantiating CuEC's ability to deplete GSH (Fig. 2d and Fig. S3 in Supporting information). The CuEC demonstrated remarkable GSH depletion properties attributed to the presence of Cu(II), which could enhance the disruption of cellular antioxidant defense mechanisms. Therefore, we subsequently assessed the chemodynamic activity of CuEC. To demonstrate the generation of ·OH, hydroxyphenyl fluorescein (HPF) was used as a probe. HPF has no fluorescence, but it can produce strong green fluorescence when reacts with ·OH. In the CuEC + GSH group, there was a significant increase in the fluorescence intensity at 515 nm of HPF, whereas the fluorescence intensity of both the control group (HPF) and the CuEC-treated group remained relatively stable. This demonstrates CuEC can effectively produce ·OH in the presence of GSH (Fig. 2e and Fig. S4 in Supporting information). The production of ·OH was further assessed by measuring the degradation of methylene blue (MB). As shown in Fig. 2f, in the absence of GSH, the intensity of the absorbance peak of MB in the CuEC-treated group remained nearly unchanged compared to that of the control group (MB only). The insignificant color change also indicates that MB was not degraded (inset of Fig. 2f). However, the addition of GSH to CuEC resulted in a significant decrease in MB absorbance and a noticeable lightening of the color. These results demonstrate that CuEC can effectively deplete GSH and achieve chemodynamic therapeutic effects.

We further investigated the TP properties of EC by testing the TP fluorescence spectra and TP absorbance cross-section in the wavelength range of 860–1000 nm. As shown in Fig. 3a and Fig. S5a (Supporting information), fluorescence emission occurred under the excitation of 860–1000 nm TP laser. Due to the higher concentration used during TPE fluorescence measurements and the fluorescence reabsorption effect, the TPE fluorescence signal exhibits a red-shift compared to OPE fluorescence under the same solvent conditions [51]. Fig. 3b illustrates a quadratic correlation

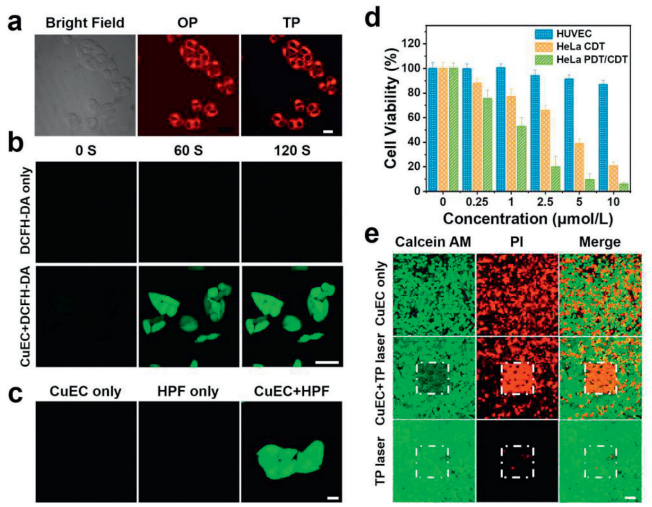

Fig. 4. (a) Fluorescent images of HeLa cells incubated with CuEC (5 μmol/L) under OP (488 nm) and TP (1000 nm) excitation. Scale bar: 20 μm. (b) Intracellular generation of ROS using DCFH-DA (5 μmol/L) as probe under 1000 nm fs laser irradiation. Scale bar: 20 μm. (c) Intracellular generation of •OH using HPF (5 μmol/L) as probe. Scale bar: 20 μm. (d) MTT assay of HUVEC and HeLa cells. (e) Calcein AM/PI co-staining analysis of HeLa cells. Scale bar: 100 μm.

between the intensity of TP fluorescence and laser power, thereby proving the TP properties of EC. Furthermore, the TP absorbance cross-section was calculated to be 6 GM at 1000 nm (Fig. S5b in Supporting information). The photostability of EC was further evaluated. As shown in Fig. 3c and Fig. S6 (Supporting information), the fluorescence intensity of EC exhibited no significant decrease after continuous irradiation with either a 488 nm laser or a 1000 nm fs laser for 10 min, suggesting that EC exhibits excellent photostability. The $^1O_2$ generation ability of CuEC was subsequently evaluated under 532 nm laser irradiation and 1,3-diphenylisobenzofuran (DPBF) as an indicator (Fig. 3d and Fig. S7 in Supporting information). The absorbance of DPBF treated with CuEC only remained unchanged under 532 nm laser irradiation, similar to the control group (DPBF only), indicating a lack of $^1O_2$ generation. However, following the addition of GSH, the absorbance of DPBF gradually decreased under the 532 nm laser irradiation, exhibiting a similar trend to that observed in the EC group. Next, the $^1O_2$ generation ability of CuEC under OP and NIR-II TP (1000 nm fs laser) irradiation was evaluated. The ESR result is consistent with that obtained under OP laser irradiation, indicating that EC can effectively generate $^1O_2$ under OP or NIR-II TP laser irradiation, which proves that CuEC can effectively produce $^1O_2$ under the excitation of OP or NIR-II TP in the presence of GSH (Figs. 3e and f). The high production of $^1O_2$ observed after CuEC interacts with GSH suggests that CuEC holds great potential for the application of TP-PDT in biological systems.

The internalization of CuEC in HeLa cells was subsequently investigated using confocal laser scanning microscopy (CLSM). In order to improve the solubility of CuEC, CuEC containing 1% DMSO was selected for subsequent cell experiments, and no significant CuEC aggregation occurred in this system (Fig. S8 in Supporting information). As shown in Fig. 4a and Fig. S9 (Supporting information), after being incubated with CuEC at 37 °C for 2 h, HeLa cells exhibited intense intracellular red emission under both OPE (488 nm) and NIR-II TPE (1000 nm fs laser), similar to cells incubated with EC (Fig. S10 in Supporting information). This indicates that the cells were able to efficiently uptake CuEC and activate it to an "ON" state. To further investigate the effect of GSH concentration on activation, we pre-treated the cells with GSH and buthionine sulfoximine (BSO, a GSH scavenger [52]), followed by incubation with CuEC. As shown in Fig. S11 (Supporting information), cells pre-treated with GSH exhibited an increase in fluorescence intensity, while fluorescence intensity was significantly reduced in cells pre-treated with BSO. The ROS generation capacity of CuEC under NIR-II TP laser irradiation was subsequently assessed by employing 2′,7′-dichlorodihydrofluorescein diacetate (DCFH-DA) *in vitro*. DCFH-DA is a fluorescent probe that exhibits a maximum emission peak at approximately 525 nm following oxidation by ROS. As shown in Fig. 4b, a gradual increase in green fluorescence was observed in HeLa cells after treatment with CuEC + DCFH-DA under NIR-II TP (1000 nm fs laser) irradiation. Conversely, no significant fluorescence increase was observed in the control group (DCFH-DA only). These findings provide evidence of the efficient ROS generation for TP-PDT under NIR-II TP irradiation. Intracellular GSH depletion was investigated using GSH assay kits. As shown in Fig. S12 (Supporting information), the intracellular GSH content of HeLa cells undergoes a significant decrease after incubation with CuEC. This not only diminishes the antioxidant capacity of the tumor cells but also generates Cu^+ as a Fenton-like reagent, which produces •OH at the cellular level. The ability of CuEC to generate •OH was detected using HPF as a probe in HeLa cells. As shown in Fig. 4c, no significant green fluorescence was observed in cells treated with HPF alone or CuEC alone. However, the co-incubation of CuEC and HPF resulted in strong green fluorescence observed in the cells, indicating that CuEC can effectively produce •OH in the presence of GSH. Given the efficient ROS generation capability of CuEC *in vitro*, a subsequent evaluation was performed to assess the therapeutic effectiveness of CuEC. The standard 3-(4,5-dimethylthiazolyl-2)−2,5-diphenyltetrazolium bromide (MTT) assay was used to investigate the therapeutic effectiveness of different concentrations of CuEC on cancer cells (HeLa cells) and normal cells (human umbilical vein endothelial cells (HUVEC)). Under dark condition, the viability of normal cells remained at approximately 90% even at a high concentration of 10 μmol/L, as depicted in Fig. 4d, thereby demonstrating the excellent biocompatibility of CuEC towards normal cells. In contrast, the viability of HeLa cells decreased significantly with the increasing concentrations of CuEC, indicating that CuEC can effectively achieve CDT on HeLa cells in dark. Additionally, the combination therapy effect of CuEC was examined. After 3 min of 532 nm laser irradiation, the viability of HeLa cells was significantly lower than that of cells treated without laser irradiation. These results indicate that the combination of PDT and CDT had a greater antitumor effect.

Next, the combination of NIR-II TP PDT and CDT effect of CuEC was further evaluated on HeLa cells using the calcein-AM (green, live cells) and propidium iodide (PI, red, dead cells) co-staining methods. As shown in Fig. 4e, the NIR-II TP laser-treated group displayed robust green fluorescence, indicating no apparent cell death. In the CuEC-treated group, both red and green fluorescence were present with similar intensity, indicating that CuEC exhibits cytotoxicity by CDT effect. To evaluate the efficiency of CuEC in TP-PDT and CDT, a square region was selected for TP laser scanning. After 3 min of 1000 nm fs laser irradiation, complete cell death was confirmed in the scanned area by the presence of red fluorescence. The experimental results demonstrate that CuEC can achieve the combination of NIR-II TP PDT and CDT in cancer cells, consistent with the MTT results.

After evaluating CuEC's therapeutic effects in a 2D monolayer model, we proceeded to investigate the biological impact of CuEC using a 3D MCTS model. The utilization of MCTS offers a more authentic portrayal of clinical tumor treatment scenarios and serves as an invaluable tissue model for investigating drug delivery [53,54]. Initially, we examined the cellular uptake of CuEC within HeLa MCTS using z-scanning CLSM. As shown in Fig. 5a, CuEC exhibits red fluorescence within the 3D MCTS under both OPE and TPE, confirming its ability to effectively penetrate the complex 3D

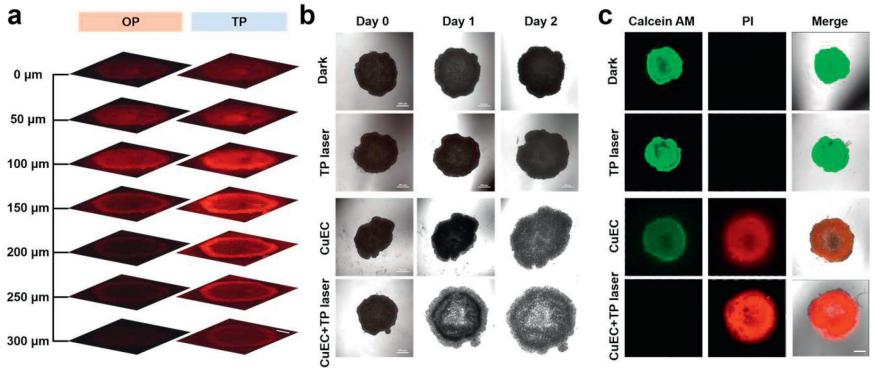

Fig. 5. (a) Fluorescent images of HeLa MCTS incubated with CuEC (5 μmol/L) under OP (488 nm) and TP (1000 nm) excitation. Scale bar: 300 μm. (b) Inhibition of tumor cells growth in HeLa MCTSs. Scale bar: 500 μm. (c) Calcein AM/PI co-staining analysis of HeLa MCTSs. Scale bar: 500 μm.

cellular structure and release EC in the presence of GSH. In the deeper regions of the MCTS, the spheres displayed more intense fluorescence when excited using TP fs laser, indicating that TP excitation provides superior resolution and deeper tissue penetration capabilities. Subsequently, we assessed CuEC's capacity to generate ROS within the MCTS under TP laser irradiation. As shown in Fig. S13 (Supporting information), a gradual increase in green fluorescence was observed in MCTS treated with CuEC + DCFH-DA under NIR-II TP (1000 nm fs laser) irradiation. The experimental results demonstrate that CuEC efficiently generates ROS within the complex 3D cellular structure under TP irradiation. Next, the efficacy of CuEC in combination therapy on MCTS was tested. As shown in Fig. 5b, after incubation with CuEC (CDT only), the structure of the MCTS became loose. In the CuEC + TP laser-treated group, not only did the MCTS exhibit reduced compactness, but it also underwent collapse and rupture in the central region. To further determine the effect of combination therapy, calcein AM and PI co-staining experiment was performed. As shown in Fig. 5c, CuEC exhibited a significant damage effect on 3D MCTS, the killing effect is more significant after irradiation by TP laser. All the experimental results demonstrate that CuEC has effective TP-PDT/CDT combination therapy effects in the 3D MCTS tumor model.

In summary, we have developed a GSH-activatable PS for combination NIR-II TP-PDT/CDT therapy. The Cu^{2+} functions as a "lock" in a normal physiological environment, inhibiting the fluorescence and $^1O_2$ generation ability of EC. However, within the TME, overexpressed GSH acts as a "key" that triggers the release of both Cu^+ and EC. The released EC can be utilized for NIR-II two-photon excitation-based fluorescence imaging and TP-PDT. Meanwhile, Cu^+ can produce highly toxic $^{\bullet}OH$ *via* Fenton-like reaction for CDT. By integrating NIR-II TP-PDT/CDT strategies, CuEC demonstrates remarkable efficacy in killing tumor cell both in 2D monolayer cells and 3D MCTS, thereby presenting a novel idea for the development of advanced theranostic agents for treatment of deep-seated tumors.

Declaration of competing interest

The authors declare that they have no known competing financial interests or personal relationships that could have appeared to influence the work reported in this paper.

CRediT authorship contribution statement

Zekun Gao: Writing – original draft, Investigation, Data curation. **Xiuli Zheng:** Writing – original draft, Project administration, Funding acquisition, Data curation. **Weimin Liu:** Investigation, Data curation. **Jie Sha:** Data curation. **Shuaishuai Bian:** Data curation. **Haohui Ren:** Data curation. **Jiasheng Wu:** Data curation. **Wenjun Zhang:** Writing – review & editing. **Chun-Sing Lee:** Writing – review & editing. **Pengfei Wang:** Writing – review & editing, Project administration, Funding acquisition.

Acknowledgments

This work was supported by the project of the National Key Research and Development Program of China (No. 2022YFA1207600), the National Natural Science Foundation of China (Nos. 62005294, 62375272), and TIPC Director's Fund.

Supplementary materials

Supplementary material associated with this article can be found, in the online version, at doi:10.1016/j.cclet.2024.109874.

References

[1] B. Yang, Y. Chen, J. Shi, Chem. Rev. 119 (2019) 4881–4985.
[2] S. Luo, C. Liang, Q. Zhang, P. Zhang, Chin. Chem. Lett. 34 (2023) 107666.
[3] Y. Nosaka, A.Y. Nosaka, Chem. Rev. 117 (2017) 11302–11336.
[4] X. Zhao, J. Liu, J. Fan, H. Chao, X. Peng, Chem. Soc. Rev. 50 (2021) 4185–4219.
[5] J.P. Celli, B.Q. Spring, I. Rizvi, et al., Chem. Rev. 110 (2010) 2795–2838.
[6] E. Ortega-Forte, A. Rovira, M. López-Corrales, et al., Chem. Sci. 14 (2023) 7170–7184.
[7] S. Wang, Z. Zhao, J. Yao, et al., Chin. Chem. Lett. 34 (2023) 107805.
[8] M. Ethirajan, Y. Chen, P. Joshi, R.K. Pandey, Chem. Soc. Rev. 40 (2011) 340–362.
[9] X. Deng, Z. Shao, Y. Zhao, Adv. Sci. 8 (2021) 2002504.
[10] L. Pang, X. Tang, L. Yao, et al., Chem. Sci. 14 (2023) 3070–3075.
[11] D. Song, S. Chi, X. Li, et al., ACS Appl. Mater. Interfaces 11 (2019) 41100–41108.
[12] L. Li, C. Shao, T. Liu, et al., Adv. Mater. 32 (2020) 2003471.
[13] Z. Zheng, H. Liu, S. Zhai, et al., Chem. Sci. 11 (2020) 2494–2503.
[14] V. Juvekar, C.S. Lim, D.J. Lee, et al., Chem. Sci. 12 (2021) 427–434.
[15] J. Wang, J. Li, Z. Yu, et al., Anal. Chem. 94 (2022) 14029–14037.
[16] Y. Shen, A.J. Shuhendler, D. Ye, J.J. Xu, H.Y. Chen, Chem. Soc. Rev. 45 (2016) 6725–6741.
[17] B. Ma, H. Xu, W. Zhuang, et al., ACS Nano 14 (2020) 5862–5873.
[18] Z. Sun, L.P. Zhang, F. Wu, Y. Zhao, Adv. Funct. Mater. 27 (2017) 1704079.
[19] X. He, B. Situ, M. Gao, et al., Small 15 (2019) 1905080.
[20] A. Jenkins, Nat. Photonics 2 (2008) 256.
[21] T.C. Pham, D.J. Lee, D.H. Kim, et al., Chem. Commun. 59 (2023) 4503–4506.
[22] K. Wen, H. Tan, Q. Peng, et al., Adv. Mater. 34 (2022) 2108146.
[23] J.N. Hao, K. Ge, G. Chen, B. Dai, Y. Li, Chem. Soc. Rev. 52 (2023) 7707–7736.
[24] X. Ma, M. Mao, J. He, C. Liang, H.Y. Xie, Chem. Soc. Rev. 52 (2023) 6447–6496.
[25] H. Xiao, G. Wu, S. Tan, X. Tan, Q. Yang, Chem. Asian J. 19 (2024) e202301036.
[26] G. Wu, F. Liu, N. Li, et al., Anal. Chem. 95 (2023) 17372–17383.
[27] G. Wu, F. Liu, N. Li, et al., Adv. Sci. 10 (2023) 2304104.
[28] J.J. Soldevila-Barreda, N. Metzler-Nolte, Chem. Rev. 119 (2019) 829–869.
[29] E. Ju, K. Dong, Z. Chen, et al., Angew. Chem. Int. Ed. 55 (2016) 11467–11471.
[30] H. Kong, Q. Chu, C. Fang, et al., Adv. Sci. 8 (2021) 2100241.
[31] E. Falcone, A.G. Ritacca, S. Hager, et al., J. Am. Chem. Soc. 144 (2022) 14758–14768.
[32] S. Wan, Q. Cheng, X. Zeng, X. Zhang, ACS Nano 13 (2019) 6561–6571.
[33] L. Zhu, Y. You, M. Zhu, et al., Adv. Mater. 34 (2022) 2207174.
[34] Q. Fan, J. Li, Y. Zhu, et al., ACS Appl. Mater. Interfaces 12 (2020) 4797–4803.
[35] S. Huang, W. Wang, J. Cheng, et al., Microchem. J. 159 (2020) 105494.
[36] Y. Zhang, Q. Jia, J. Li, et al., Adv. Mater. 35 (2023) 2305073.
[37] H. Wang, J. Guo, W. Lin, et al., Adv. Mater. 34 (2022) 2110283.

[38] Q. Zeng, X. Li, S. Xie, D. Xing, T. Zhang, Biomaterials 290 (2022) 121867.
[39] C. Li, Y. He, L. Ou, et al., Chin. Sci. Bull. 51 (2006) 1050–1054.
[40] X. Wang, Z. Sun, W. Liu, H. Zhang, J. Shandong Univ. Technol. (Sci. Technol.) 17 (2003) 21–24.
[41] Q. Zhao, H. Zhang, Nat. Prod. Commun. 3 (2008) 1701–1704.
[42] J. Liu, Y. Zhao, J. Zhao, et al., J. Photochem. Photobiol. B 68 (2002) 156–164.
[43] G. Li, H. Wang, R. Zhu, et al., J. Nat. Prod. 75 (2012) 142–147.
[44] Y. Sun, Y. Hou, Q. Zhou, et al., Inorg. Chem. 49 (2010) 10108–10116.
[45] L. Lin, T. Huang, J. Song, et al., J. Am. Chem. Soc. 141 (2019) 9937–9945.
[46] J. Liu, Y. Yuan, Y. Cheng, et al., J. Am. Chem. Soc. 144 (2022) 4799–4809.
[47] W. Jin, Z. Chen, Y. Wang, et al., Chin. Chem. Lett. 35 (2024) 109328.
[48] Z. Diwu, L. Jiang, M. Zhang, Sci. China B 33 (1990) 18–26.
[49] V.V. Volchkov, V.L. Ivanov, B.M. Uzhinov, J. Fluoresc. 20 (2010) 299–303.
[50] Y. Liu, W. Zhen, L. Jin, et al., ACS Nano 12 (2018) 4886–4893.
[51] X. Yang, D. Zhang, J. Li, et al., Chem. Commun. 56 (2020) 9032–9035.
[52] L. Zeng, S. Kuang, G. Li, et al., Chem. Commun. 53 (2017) 1977–1980.
[53] B. Li, H. Cao, J. Zheng, et al., ACS Appl. Mater. Interfaces 13 (2021) 9739–9747.
[54] S. Kuang, F. Wei, J. Karges, et al., J. Am. Chem. Soc. 144 (2022) 4091–4101.